

## SYNTHESIS OF CARBON NANOSHEETS USING MICROWAVE PLASMA ENHANCED CHEMICAL VAPOR DEPOSITION SYSTEM

**Chang Soon Huh**

Applied Chemistry Major, Division of  
Chemical and Environmental  
Engineering, College of Engineering /  
Dong-eui University, **South Korea**  
0411black@deu.ac.kr

### ABSTRACT

Petal-like graphite nano sheets were synthesized by acetylene gas in a hydrogen plasma environment using Microwave Plasma Enhanced Chemical Vapor Deposition (MPECVD) equipment. The "Petal" - like structure is arranged vertically with sharp graphite tips and horns, and the thin edges potentially have potential as field emission devices. As the reaction time increased and the temperature decreased, the size of "petal" was observed to increase. Despite the high energy of the plasma, the formation of carbon nanotubes could not be confirmed in the upper experiments, but the remarkable growth of carbon nanotubes was confirmed after controlling the reaction temperature. In order to investigate the optimal conditions for growth of carbon nano sheets, the reaction times were changed at various temperatures under hydrogen atmosphere.

**Keywords:** Carbon nano sheets, MPECVD, Ni thin films, growth rate.

### INTRODUCTION

Carbon nanotubes were discovered by Iijima in 1991 [1]. He observed that nanotubes of graphite were deposited on the negative electrode during the direct-current arcing of graphite for the preparation of fullerenes. Nanotubes are composed entirely of  $sp^2$  bonds, similar to those of graphite [2]. This bonding structure, stronger than the  $sp^3$  bonds found in diamond, provides the molecules with their unique strength. Nanotubes naturally align themselves into "ropes" held together by van der Waals forces [3]. These nanotubes are concentric graphitic cylinders closed at either end due to the presence of five-membered rings. Nanotubes can be multiwall with a central tubule of nanometric diameter surrounded by graphitic layers separated by  $\sim 3.4 \text{ \AA}$  [4]. Unlike the multi-walled nanotubes (MWNT), in single-walled nanotubes (SWNT) there is only the tubule and no graphitic layers. The simplest possible single-walled carbon nanotubes can be visualized by cutting the  $C_{60}$  structure across the middle and adding a cylinder of graphite of the same diameter [5]. If  $C_{60}$  is bisected normal to a five-fold axis, an armchair tube is formed, and if it is bisected normal to a three-fold axis, a zigzag tube is formed. Armchair and zigzag tubes are achiral. In addition to these, a variety of chiral tubes can be formed with the screw axis along the axis of the tube. According to the accepted "Russian doll" model, nanotubes consist of graphite layers rolled up into closed concentric cylinders [6]. In contrast to the previous model, "scroll" model, in which a single graphite sheet, possibly containing dislocation defects, is rolled up to form a multiwall tube.

## EXPERIMENTAL AND THEORETICAL METHODS

Microwave plasma is sustained in the frequency of 2.45 GHz power supply. Microwave-excited plasmas have two appealing properties: If applied in surface-wave-sustained mode, they are especially well suited to generate large-area plasmas of high plasma density. In addition, both in surface-wave and resonator mode, they can exhibit a high degree of spatial localization. This allows to spatially separating the location of plasma generation from the location of surface processing. In trivial microwave plasmas, the electric field strength is about  $E_0 \sim 30$  V/cm and the maximum electron amplitude ( $x$ ) is less than  $10^{-3}$  and the highest electron energy in one cycle is about 0.03 eV. In this degree energy is insufficient of plasma sustaining so the microwave discharge in a low pressure ( $< 1$  Torr, less than DC/RF discharge) is problematic. Microwave absorption degree depends on the pressure, because it is a function of the collision frequency between electron and neutron species. In the case of 2.45 GHz microwave frequency, the effective microwave absorption has done at 5 ~ 10 Torr Helium pressure. The effective pressure of other gases are 0.5 ~ 10 Torr. Short wavelength (2.45 GHz corresponding to 12.24 cm) microwave plasma has local high density in a small portion and the rapid decrease of plasma density in the surrounding. The power transfer to the plasma is done through the microwave applicators - waveguide, resonance cavity, coaxial applicator. The dielectric materials (quartz, alumina and so on) separate the plasma from the microwave. In a surface wave (SW) discharge the plasma column is sustained by the field of a guided wave that propagates along the plasma column and the dielectric containing the plasma; these media form the sole propagating and guiding structure, that is, no other wave guiding structure is required. The SW can be launched from a localized, small size exciter whose axial length can be very small compared to the plasma column length. This length is and increasing functional of the HF power delivered to the launcher. We ignited hydrogen plasma because it particles the metal thin film and removes the amorphous carbon contamination. Parchen's law (eq. 1) let us know the breakdown voltage of a gap is a non-linear function of the product of the gas pressure and the gap distance [7].

$$V = f(pd) \quad (1)$$

( $p$  and  $d$  are pressure and gas distance, respectively)

Figure 1 shows the schematic diagram of this MPECVD experimental setup. The microwave source frequency is 2.45 GHz and continuous power output up to 1200 W. The circulator allows the power to go from the microwave source to the load but prevents power reflected by the load from reaching the source again, thus preventing the magnetron from overheating. The three-stub tuner is a waveguide component used to match the load impedance and minimizes the amount of reflected power, which results in the most efficient coupling of power to the load. A quartz tube which forms the reaction chamber passes through this cavity and reaction gasses are introduced from one end and exhausted at the other end. Temperature is measured by an R-type thermocouple which is shielded by a ceramic tube and positioned at the outer surface of the 25.4 mm outer diameter quartz tube. For the reliable experiment, we changed the quartz tube in each experiment. System divided two zones and named as 1 and 2. The zone 1 applied to a reactive chamber of petal-like graphite synthesizer and the zone 2 used for CNTs synthesizer. Petal-like graphite sheets are entirely attributed to the plasma energy but when we grow CNTs, the controlled thermal energy is key factor. Single-zone electrical furnace (hot-wall type, temperature controllable up to 1000 °C) installed horizontally next to zone 1. Most of the experiments were done in a low vacuum

circumstance (roughing pump, maximum to  $1 \times 10^{-2}$  torr). Vacuum system consists of the metering valve which applied to control the reaction pressure and the pirani gauge (Leybold, Thermovac TM20) and the capacitance manometer (MKS, Baratron type 626A). The carrier-gas controlled by MFCs (MKS, type 1179) and exhaust gas flow into the LN<sub>2</sub> trap for protecting the rotary pump.

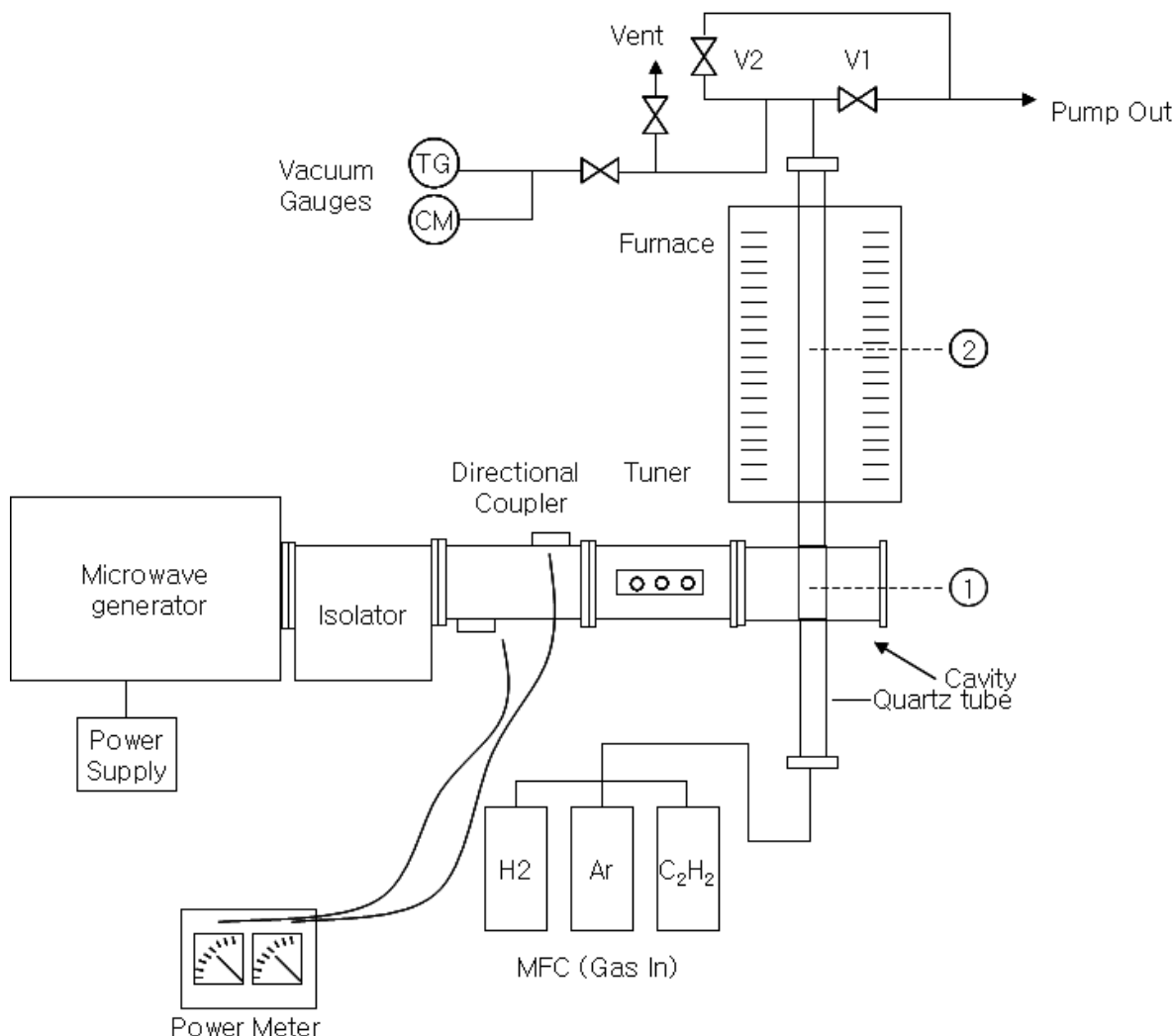


**Figure 1. MPECVD system. Cavity for petal-like nano sheets synthesizes (1), and cavity for CNTs growing (2).**

\* **TG: Thermocouple Gauge.**

**CM: Capacitance manometer.**

And we discuss techniques that have the common objective of structurally characterizing films and surfaces. The characterization of thin films and surfaces can be divide two methods, structural characterization analysis and chemical characterization analysis. The structural analysis includes optical, electron, and scanning probe microscopes. Thus the scanning electron microscope (SEM) would primarily be used to obtain the required information of surface topography and microstructure and the transmission electron microscope (TEM) is indispensable for the high resolution lattice images of both plan-view and transverse film sections. And finally to confront structural information required of substrate and film surfaces there is the atomic force microscope (AFM) and the scanning tunnelling microscope (STM).

In this section, we deal with two major structural characterization methods and summarize major chemical characterization techniques in Table 1.

**Table 1. Summary of major chemical characterization techniques [8].**

Method	Elemental sensitivity	Detection limit (at. %)	Lateral resolution	Effective probe depth
Scanning electron microscope/energy dispersive X-ray (SEM/EDX)	Na-U	~0.1	~1 $\mu$ m	~1 $\mu$ m
Auger electron spectroscopy(AES)	Li-U	~0.1-1	500 Å	15 Å
X-ray photoelectron spectroscopy(XPS)	Li-U	~0.1-1	~100 $\mu$ m	15 Å
Rutherford backscattering(RBS)	He-U	~1	1mm	~200 Å
Secondary-ion mass spectrometry(SIMS)	H-U	10 <sup>-4</sup>	~1 $\mu$ m	15 Å

### SEM (Scanning electron microscope)

First, we must define the distinction between the SEM and TEM. The latter is a true microscope in that all image information is acquired but in the SEM, only a small portion of the total image is probed at any instant and the image builds up serially by scanning the probe. Upon impinging on the specimen, the primary electrons decelerate and in losing energy, transfer it in elastically to other atomic electrons and to the lattice. Through continuous random scattering events the primary beam effectively spreads and fills a teardrop-shaped interaction volume (Figure 2a) with a multitude of electronic excitations. The result is a distribution of electrons which manage to leave the specimen with an energy spectrum shown schematically in (Figure 2b). The most common imaging mode relies on detection of very lowest portion of the emitted energy distribution, the secondary electrons. Their very low energy means they originate from a subsurface depth of no larger than several angstroms. Resolution specifications quoted on research-quality SEMs are less than 2 nm. Great depth of focus enables images of three-dimensional to be obtained from non-planar surfaces. The contrast variation obtained can be understood with reference to Figure 2c. Sloping surfaces produce a greater secondary electron yield because the portion of the interaction volume projected on the emission region is larger than on a horizontal surface. Backscattered electrons are the high-energy as the incident electrons. The probability of backscattering increases with the atomic number  $Z$  of the sample material. An SEM is like a large X-ray vacuum tube used in conventional X-ray diffraction systems. In the process, X-rays characteristic of atoms in the irradiated area are emitted.

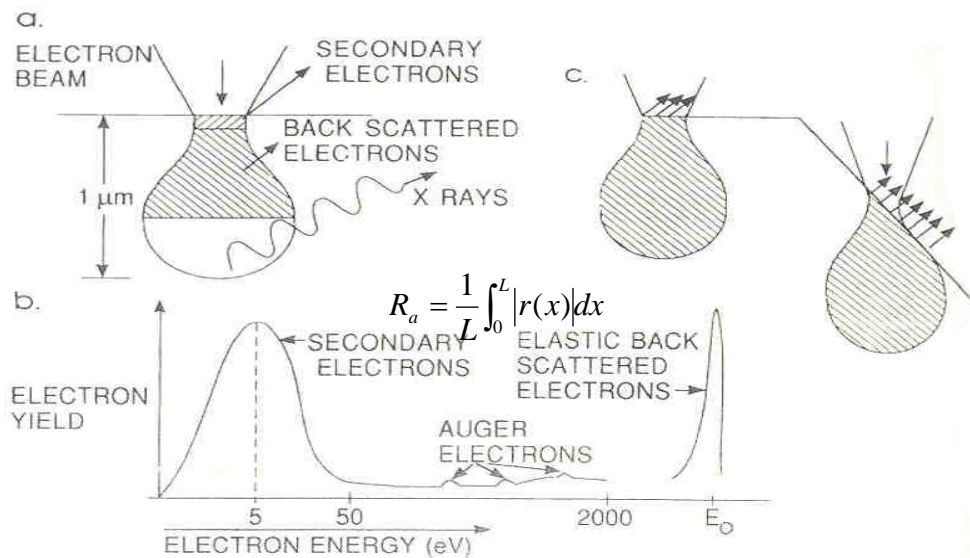


**Figure 2. Scheme of the electron emission process. (a) Electron and photon signals emanating from tear-shaped interaction volume during electron-beam impingement on specimen surface. (b) Energy spectrum of electrons emitted from specimen surface. (c) Effect of surface topography on electron emission [9].**

AFM (Atomic force microscopy)

The atomic force microscope (AFM) probes the surface of a sample with a sharp tip, a couple of microns long and often less than 100 Å in diameter. Forces between the tip and the sample surface cause the cantilever to bend, or deflect. In the analysis of the AFM data, we must consider the roughness calculation. In our experiment, the average roughness ( $R_a$ ) is used as roughness parameter because of the long history of parameter in surface finish measurement. The average roughness is the area between the roughness profile and its mean line, or the integral of the absolute value of the roughness profile height over the evaluation length:

$$R_a = \frac{1}{L} \int_0^L |r(x)| dx \quad (2)$$

When evaluated from digital data, the integral is normally approximated by a trapezoidal rule:

$$R_a = \frac{1}{N} \sum_{n=1}^N |r_n| \quad (3)$$

In Figure 3, the average roughness is the area (shown below) between the roughness profile and its centres line divided by the evaluation length (normally five sample lengths with each sample length equal to one cut off).

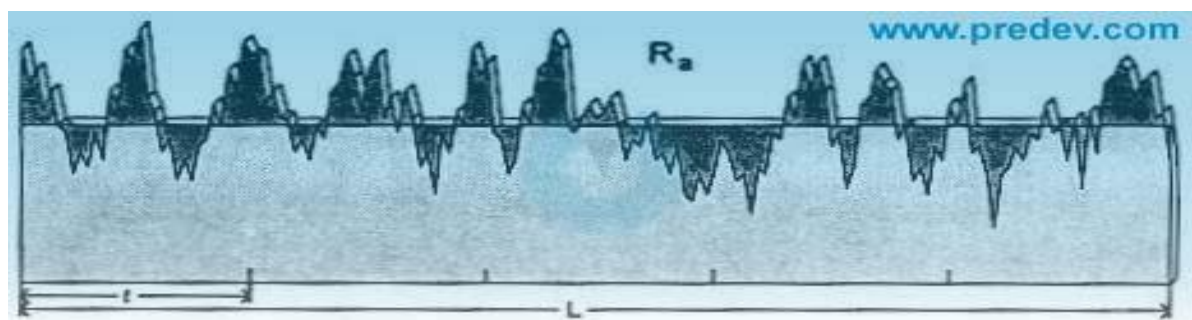


**Figure 3.** The average roughness ( $R_a$ ) is an integral of the absolute value of the roughness profile. It is the shaded area divided by the evaluation length;  $L$ .  $R_a$  is the most commonly used roughness parameter [10].

## RESULTS

We pyrolyzed benzene for a carbon source because of its high proportion of carbon. Bulk carbon source deposited on the substrate which made another form of the graphite. And the rapid temperature increase made the disordered structures. At first, carbon source was fed in by passing Ar (flow rate 100 sccm) through liquid hydrocarbons and  $H_2$  (100 sccm) was flowed for the plasma discharge. P-type Si wafer (100) placed at the center of cavity as a substrate without any pretreatments (Figure 1-1). In the low vacuum circumstance (120 mTorr),  $H_2$  fed first to make  $H_2$  plasma environment thereafter benzene was flowed into the cavity as a carbon source by bubbling for 10 min. After the reaction, we gathered the samples and examined them with various optical and spectral analyze. To confirm the presence of significant deposition, we first analyzed the morphology with HR-SEM (Hitachi S-4200, accelerating voltages 0.5-30kV). For the confirmation of crystallization, the sample was sonicated in ethanol and checked it using TEM (JEOL 2011, accelerating voltage range 80~200 kV). In the same environment except reaction times, the petal-like graphite confirmed by HR-SEM images analyzed by Laser Raman Spectrophotometer (Coherent, Innova 90-5/Spex, Ramalog 9I) at 100 mW power, 514.532 excitation line.

## DISCUSSION

From the HR-TEM image (Figure 4) we can see few graphene sheets surrounded by amorphous carbons and the edge of the tip has more graphitized crystalline structure.

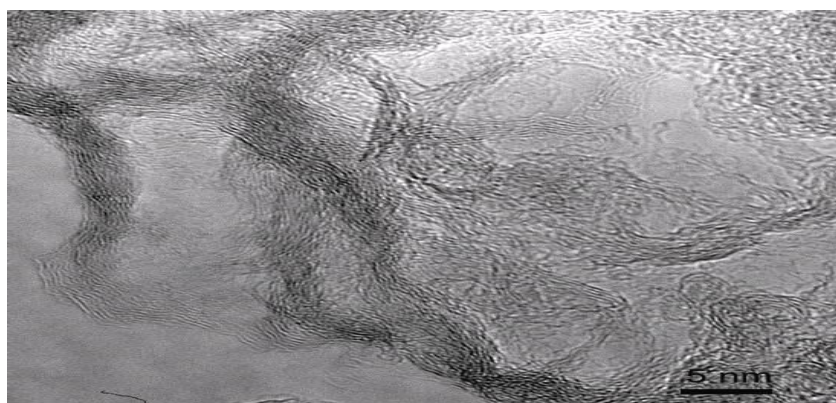


**Figure 4.** HRTEM image of Figure 5. This shows the disconnected nano sheet layers.

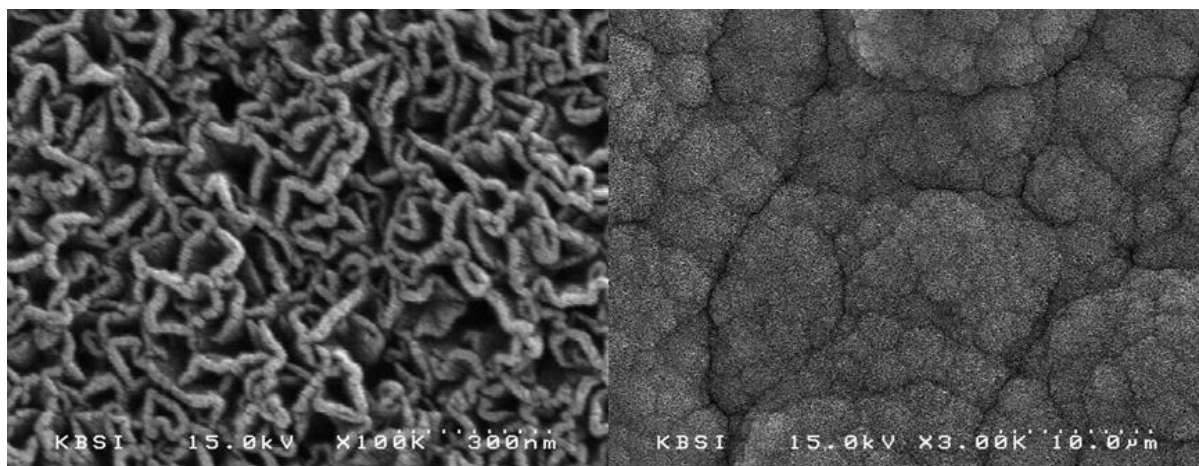


**Figure 5.** SEM image of petal-like nano sheets (right) and its magnified image (left). The condition is  $H_2$  100sccm and  $C_6H_6$  10 sccm with 400W power.

From a Raman data, we can get the same result of the low crystallinity with a disordered graphene structure. With an increment of the reaction time, it turned to glassy carbon structure from PAHs (Poly aromatic hydrocarbons) structure. The reason is easily deduced from the Raman spectra. Figure 6 shows Raman spectra of graphite sheets for 3 different synthesis times (2, 3 and 5 min; petal-like graphite sheets only showed in 5 min).

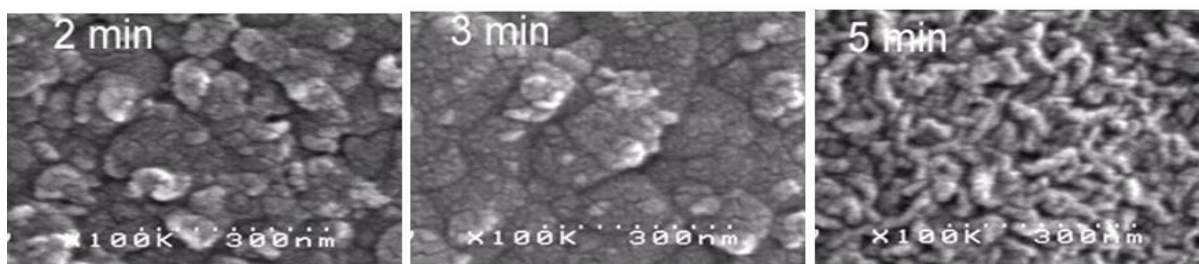
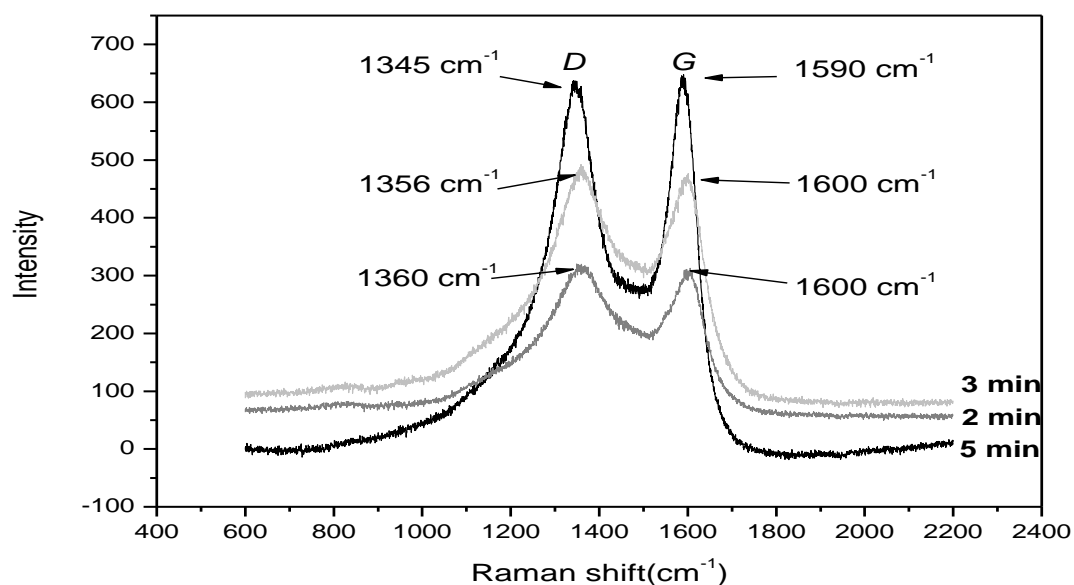
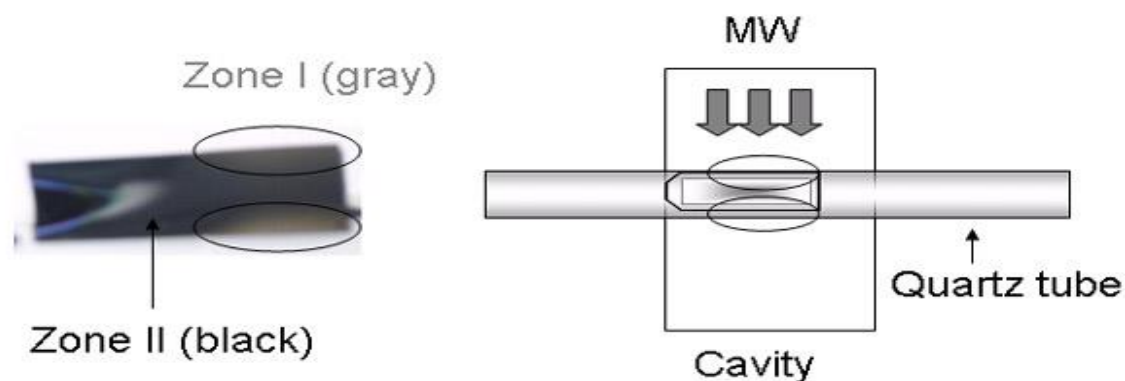


**Figure 6.** Raman data of petal-like nano sheets (top) and the corresponding HR-SEM images (bottom).

The Raman spectrum shows two strong peaks at  $1350$  and  $1590\text{ cm}^{-1}$ , with assignment as the D- and G-peak. The 2 and 3 min synthesis times show the typical PAHs spectrum which exhibits partially overlapped peaks, but the D-peak and G-peak are relatively resolved in 5 min reaction time than others. We compared the FWHM (Full width at half maximum, the peak fitted with Gaussian curve) of the G peak and D peak by the reaction time in the Raman spectrum. In the 2 min reaction time, the Raman spectrum with broad D peak (FWHM =  $163\text{ cm}^{-1}$ ) and broad G peak (FWHM =  $103\text{ cm}^{-1}$ ) and in the 3 min reaction time, FWHM (D) =  $165\text{ cm}^{-1}$  and FWHM (G) =  $104\text{ cm}^{-1}$ . In the 5 min reaction time experiment, the D peak (FWHM =  $135\text{ cm}^{-1}$ ) and G peak (FWHM =  $84\text{ cm}^{-1}$ ) are sharper than 2 and 3 min experiments. This result reveals that the structure of graphite sheets shows ordered pattern with the increment of reaction time. We also compared the  $I(D) / I(G)$  as the ratio of peak heights and the samples 5, 3, 2 min show the same  $I(D) / I(G)=1$ . A. C. Ferrari et al. suggested the three-stage model [11], and our results are in the transition state from graphite nanocrystalline graphite stage. E. Cappelli et al. introduced the effect of temperature on the morphology and structural properties of carbon films [12]. The D( $1350\text{ cm}^{-1}$ ) and G( $1580\text{ cm}^{-1}$ ) peak changed as a function of substrate temperature, correlated to aromatic ring formation and cluster condensation. The sharpening and increment of the  $I(D) / I(G)$  ratio come from the ordering phenomena of the aromatic rings into small graphene layer and nano-graphite particles. When we compare the samples with the HR-SEM images, the petal-like graphite sheets are deposited after the macroscopic particle aggregated carbon films. Since the petal-like graphite sheets only exist after 10 min reaction, it seems that the carbon film helps the deposition of petal-like graphite sheets and the formation of the carbon film will be the



prerequisite.

**Figure 7. The optical image of petal-like nano sheets deposited Si substrate. We defined “Zone I” (colored gray) and “Zone II” (colored black).**

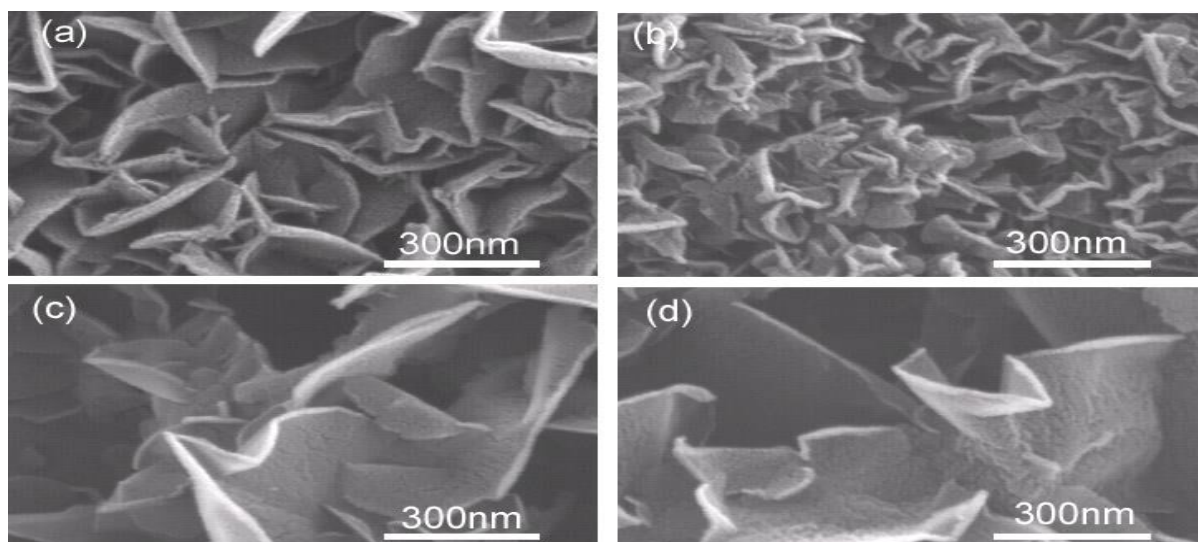
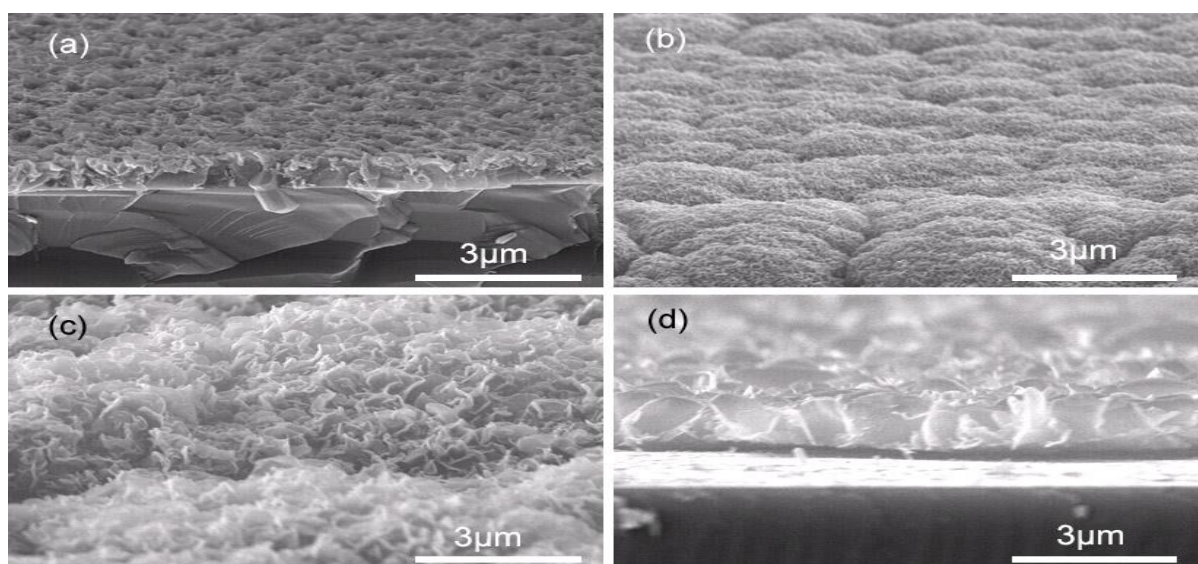


**Figure 8.** HR-SEM images of “petal”-like nano sheets. The condition was  $H_2$  100 sccm and  $C_2H_2$  10 sccm with 400 W. The reaction time was 20 min (a), (c) and 10 min (b), (d). The optical images of (a), (b) colored as gray (“Zone I”) and (c), (d) colored as black (“Zone II”). And the bottom images are tilted  $30^\circ$  angles of the same samples.



In the second experiment, we changed carbon source from benzene to acetylene. Si(100) wafer was transferred in air to the growth chamber and pumped to vacuum in flowing hydrogen at a pressure of 2.5 Torr. A 400 W microwave plasma was then turned on, and the acetylene added to start the petal-like graphite growth. Total gas flow rates of acetylene ( $C_2H_2$ ) and hydrogen ( $H_2$ ) were controlled at 100 sccm, and the mass flow ratio of  $C_2H_2$  over  $H_2$  fixed at 6%. We analyzed the morphology with HR-SEM at 10 min, 20 min reaction time (Figure 8). After the deposition of carbon materials, the top image of the Si (100) substrate which was under the intensified  $H_2$  plasma ball (we defined it as “Zone I”) colored bright gray and another part which was under the intensified plasma ball (we defined it as “Zone II”) colored black (Figure 7). We separated the sample from an optical image and compared the portions with HR-SEM results (Figure 8). The synthesis condition varied by reaction time 10 min, 20 min and they show the same multiform deposition parts as Figure 7. Under “Zone II”: (a), and (b) show the small size petals than “Zone I”: (c), and (d). Because of the microwave property, we could not use the high-temperature thermometer (it must be

designed to fit for microwave-shielding), but we can presume that the temperature of the intensified plasma ball must be over 1000 °C and another zone must be 400~600 °C from the many researches on the microwave plasma treatment. Nano-graphite petal-like nano sheets structures vertically oriented with sharp graphite tips and cones. Their very sharp and thin edges which are perpendicular to substrates can be potentially good electron field emission sites. If it is possible to control the shape of the petal, we could also control the property of the graphite sheets. From this experiment we know that the petal size increased as lowering the reaction temperature and as enlarging the reaction time. We concluded that the alignment was a plasma induced effect that the electric field in the plasma sheath formed around objects which guided the growth of the nanotubes perpendicularly from the object. We expecting the formation of petal-like nano sheets come from a plasma inductive effect.

## CONCLUSIONS

The petal like carbon nano sheets have been deposited by tubular MPECVD system on Si substrates in well-controlled manner without catalyst. The carbon nano sheets were nucleated at the fine-textured structure on the Si and grew with the increase in growth time. The reaction time is found to have a strong effect on the structure and morphology of these petal-like carbon nano sheets. The growth morphology is found to be influenced by the reaction time on to surface pattern. Improved alignment of the sharp edges of petals normal to the substrate, increased density, reduced size (geometrical enhancement factor) and solicitations between Si substrate and sheets are found to be important factors contributing to the Raman characteristics of carbon nano sheets. The height of carbon nano sheets increased proportionally to the reaction time, in contrast to the previous studies, indicating a different growth mechanism.

## ACKNOWLEDGEMENTS

This research did not receive any specific grant from funding agencies in the public, commercial, or not-for-profit sectors.

## REFERENCES

- [1] S. Iijima. (1991) Helical microtubules of graphitic carbon. *Nature*, 354, 56-58.
- [2] Wang, X. Li, Qunqing. Xie, Jing. Jin, Zhong. Wang, Jinyong. Li, Yan. Jiang. Kaili. Fan, Shoushan. (2009) Fabrication of Ultralong and Electrically Uniform Single-Walled Carbon Nanotubes on Clean Substrates. *Nano Letters*, 9 (9), 3137–3141.
- [3] R. Saito, G. Dresselhaus and M. Dresselhaus. (1998) *Physical Properties of Carbon Nanotubes*. Imperial College Press.
- [4] Yoshinori Ando, Xinluo Zhao, Kaori Hirahara, Kazutomo Suenaga, Shunji Bandow and Sumio Iijima. (2000) Mass production of single-wall carbon nanotubes by the arc plasma jet method. *Chem Phys Lett*, 323 (5-6), 580.
- [5] Sugai T, Omote H, Bandow S, Tanaka N and Shinohara H. (2000) Syntheses of single- and double-wall carbon nanotubes by the HTPAD and HFCVD methods. *J Chem Phys.*, 112 (13), 6000.
- [6] M. Hiramatsu and M. Hori. (2006) Fabrication of Carbon Nanowalls Using Novel Plasma Processing. *Jpn. J. Appl. Phys.*, 45.
- [7] Merriam-Webster Online Dictionary. Merriam-Webster, Inc. (2013) Retrieved June 9, 2017.
- [8] M. Ohring. (2002) *Materials Science of Thin Films 2nd Ed*: Academic Press, San Diego.

- [9] N. G. Shang, F.C.K. Au, X.M. Meng, C. S. Lee, I. Bello, S. T. Lee. (2002) Microstructure and field emission properties of coral-like carbon nanotubes. *Chem. Phys. Lett.*, 358, 187.
- [10] A. C. Ferrari, J. Robertson. (2000) Interpretation of Raman spectra of disordered and amorphous carbon. *Phys Rev B* , 61, 14095
- [11] E. Cappelli., S. Orlando., G. Mattei., C. Scilletta., F. Corticelli., P. Ascarelli. (2004) Nano-structured oriented carbon films grown by PLD and CVD methods. *Appl. Phys. A*, 79, 2063.
- [12] C. Bower, W. Zhu, S. Jin, O. Zhou. (2000) Nucleation and growth of carbon nanotubes by microwave plasma chemical vapor deposition. *Appl. Phys. Lett.*, 77, 830.